A workshop on atmospheric boundary layer processes

Howard University Beltsville Campus

Meteorological boundary layer one-dimensional models

Instructor: Jose D. Fuentes (jdfuentes@psu.edu)

Contents

Goals

- Learn the basic thermodynamic attributes of the convective atmospheric boundary layer.
- Investigate the salient processes influencing the thermodynamics of the convective atmospheric boundary layer.
- Apply basic methods of determine the depth of the convective atmospheric boundary layer.

Expected outcomes

- Participants will identify the key attributes of the convective atmospheric boundary layer.

- Participants will gain knowledge of the atmospheric processes exerting the greatest influences on the growth of the depth of the convective atmospheric boundary layer.
- Participants will develop skills to develop numerical models to determine temporal variations in the depth of the convective atmospheric boundary layer.

Readings

American Meteorological Society (2017). Glossary of Meteorology. http://glossary.ametsoc.org/wiki/.

Betts, A. (1973). Non-precipitating cumulus convection and its parameterization. Quarterly Journal of the Royal Meteorological Society, 99:178–196.

DeLonge, M. and Fuentes, J.D. (2012). Controls on Boundary-Layer Thermodynamics and Dynamics in Coastal West Africa During the Rainy Season of 2006. Boundary-layer meteorology, 145: 113-130.

Driedonks, A. (1982). Sensitivity analysis of the equations for a convective mixed layer. Boundary-Layer Meteorology, 22:475–480.

Lilly D.K. (1968). Models of cloud-topped mixed layers under a strong inversion. Quarterly Journal of the Royal Meteorological Society, 94: 292-309.

McNaughton, K.G. and Spriggs, T.W. (1986). A mixed-layer model for regional evaporation. Boundary-Layer Meteorology, 34: 243-262.

Tennekes, H. (1973). A model for the dynamics of the inversion above a convective boundary layer. Journal of the Atmospheric Sciences, 30:558–567.

Tennekes, H. and Driedonks, A.G.M. (1981). Basic entrainment equations for the atmospheric boundary layer. Boundary-Layer Meteorology, 20(4): 515-531.

Concepts and symbols

- Specific humidity (q) is the ratio of mass of water vapor (m_V) to total mass of air (m_V + mass of dry air, m_d) in a given volume. In mathematical form, q is defined as shown below.

$$q = \frac{m_V}{m_d + m_V} \tag{1}$$

- Virtual temperature (T_V) is the temperature that dry air would have if its pressure and density were equal to those of a given sample of moist air. The T_V is derived from the ideal gas law and uses air temperature (T) and q as shown below.

$$T_V = T \times [1 + 0.61q] \tag{2}$$

- Potential temperature (θ) is temperature that an unsaturated air parcel of dry air would have if brought dry adiabatically to its initial state or to a standard pressure. The θ is calculated based on the reference pressure (P_0) and pressure at a given height (P_z) and absolute temperarure (T_K) as shown below.

$$\theta = \left(\frac{P_0}{P_z}\right)^{\frac{R_a}{C_P}} \tag{3}$$

  Where R_a is the ideal gas law constant for moist air and C_P is the specific heat of [moist] air at constant pressure.

- Virtual potential temperature (θ_V) is the theoretical potential temperature of dry air that would have the same density as moist air. The θ_V is calculated using the equation provided below.

$$\theta_V = \theta \times [1 + 0.61q] \tag{4}$$

- Virtual sensible heat flux density (H_V) is the amount of energy flow per unit area per unit time. Using the eddy covariance concept, the H is defined interms of the volumetric heat capacity ($= \overline{\rho} C_P$, $\overline{\rho}$ is the temporarily averaged air density) and vertical velocity (w') and θ_V' covariances. The overbar denotes a temporal average, ordinarily takes over 30-minute intervals.

$$H_V = \overline{\rho} C_P \left(\overline{w'\theta'_V}\right) \tag{5}$$

- Kinematic virtual heat flux ($(\overline{w'\theta'_V})$) is the amount of energy flux density divided by the volumetric heat capacity, expressed in the units of K m s^{-1}.

- Latent heat flux density (LE) is the amount of energy associated with evaporation, transpiration, or evapotranspiration of water. The LE can be derived from edy coavariance measurements as shown below.

$$LE = L_V \overline{\rho} \left(\overline{w'q'}\right) \tag{6}$$

- Kinematic water vapor flux ($(\overline{w'q'})$) is the ratio of latent heat flux density to the product of latent heat of vaporization (L_V) and average air density ($\overline{\rho}$).

- Eddy diffusivity for momentum transfer (K_M) expresses a measure of momentum exchange between the atmosphere and the surface or between adjacent air layers. The K_M values change with time of day and height.

- Friction velocity (u_*) is shear-stress velocity and is determined as the square root of the the shear stress of the fluid air divided by the average density. The u_* can be estiamted based on eddy covariance measurments, using turbulence measurements of zonal(u), meridional (v), and vertical velocity (w) as shown below.

$$u_* = \left[\left(\overline{u'w'}\right)^2 + \left(\overline{v'w'}\right)^2\right]^{\frac{1}{4}} \tag{7}$$

- Convective velocity (W_*) is the updraft speed of convective thermals associated in the convective mixed layer. It is also known as the convective velocity scale. The w_* can be determined based on knowledge of air buoyancy ($g/\overline{\theta_V}$, g is the acceleration due to graviation), the kinematic virtual heat flux at the surface ($(\overline{w'\theta'_V})_{sfc}$), and depth of the convective mixed layer (Z_i) as shown below.

$$W_* = \left[\frac{g}{\overline{\theta_V}}(\overline{w'\theta'_V})_{sfc} Z_i\right]^{\frac{1}{3}} \tag{8}$$

- Turbulent kinetic energy (TKE) budget provides the relative contributions of physical processes (e.g., wind shear, buoyancy) contributing to turbulent flows.
- Obukhov length (L) is used to describe the effects of buoyancy versus mechanical forces on turbulent flows in the atmospheric surface layer. The L is calculated showing the equation listed below.

$$L = -\frac{u_*^3/k}{\frac{g}{\overline{\theta_V}}(\overline{w'\theta'_V})_{sfc}} \tag{9}$$

  Negative values correspond to unstable conditions whereas posive values apply to stable conditions. Note that when $(\overline{w'\theta'_V})_{sfc}$ approaches zero then L is undefined, which can occurred during the night-to-day and day-to-night transition periods.

- Monin–Obukhov similarity theory (MOST) describes the universal relationships for atmospheric surface layer wind and scalar profiles in stratified flows.
- Atmospheric static stability refers to the ability of an air parcel at rest to become turbulent or laminar due to the effects of buoyancy.
- Atmospheric dynamic stability is produced through the horizontal movement of air and the physical forces it is subjected to such as the Coriolis force and pressure gradient force.

Theoretical background

The concepts outlined in this document apply to the convective atmospheric boundary layer (see Figure 1). The principal goal of this write-up is to provide the basic theory of numerical models to estimate the depth of the convective atmospheric boundary layer. Several numerical models are introduced to study the convective boundary layer, focusing on the one proposed by McNaughton and Spriggs (1986). Based on the conservation of energy (DeLonge and Fuentes 2012), the rate of change of mixed layer virtual potential temperature ($\partial\theta_{V_m}/\partial t$) can be determined by knowing the advection of energy, changes in kinematic heat flux across the landscape of interest, and the vertical transfer of kinematic heat as shown in Equation 10.

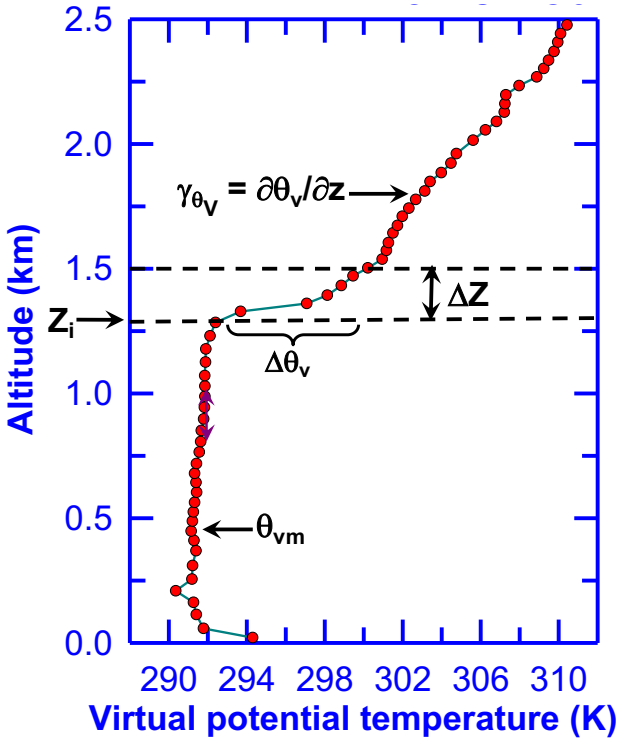

Figure 1: This figure illustrates the thermodynamic state of the convective atmospheric boundary layer during the middle of a sunny day. The vertical variation of virtual potential temperature (θ_V) with altitude (Z) is shown with red circles connected to green lines. The mixed layer virtual potential temperature (θ_{V_m}), depth of the mixed layer (Z_i), strength of thermal inversion at the top of the mixed layer ($\Delta\theta_V$), and temperature gradient above the mixed layer (γ_{θ_V}) are also shown.

$$\frac{\partial\theta_{V_m}}{\partial t} + \overline{u}\frac{\partial\theta_{V_m}}{\partial x} = -\frac{\partial\left(\overline{u'\theta'_V}\right)}{\partial x} - \frac{\partial\left(\overline{w'\theta'_V}\right)}{\partial z} \tag{10}$$

where $\overline{u}$ is the mean wind speed assumed along the prevailing wind direction, ($\overline{u'\theta'_{V_m}}$) and ($\overline{w'\theta'_{V_m}}$) are the horizontal and vertical kinematic heat fluxes, respectively. In the horizontally homogeneous atmospheric convective boundary layer (i.e., $\partial\left(\overline{u'\theta'_V}\right)/\partial x = 0$), the advection can be neglected. Under such assumptions, the integration of the simplified conservation of energy, from the surface to the depth of the mixed layer (Z_i), yields Equation 11 (Tennekes 1973, Betts 1974).

$$Z_i\frac{\partial\theta_{V_m}}{\partial t} = \left(\overline{w'\theta'_V}\right)_{sfc} - \left(\overline{w'\theta'_V}\right)_{Z_i} \tag{11}$$

In this model (Equation 11), in the absence of condensation processes and regional subsidence, the θ_{V_m} varies in response to the kinematic heat input from the surface ($(\overline{w'\theta'_V})_{sfc}$) and from above the mixed layer ($(\overline{w'\theta'_V})_{Z_i}$). This input of energy from aloft and surface governs the growth rate of the convective mixed layer. Additionally, the $\partial\theta_{V_m}/\partial t$ in conjunction with the virtual potential temperature gradient above the mixed layer ($\gamma_{\theta_V} = \partial\theta_V/\partial z$) exert control on growth rates of the mixed layer ($\partial Z_i/\partial t$), as shown in Equation 12 (Driedonks 1982).

$$\frac{\partial Z_i}{\partial t} = \frac{1}{\gamma_{\theta_V}} \frac{\partial \theta_{V_m}}{\partial t} \tag{12}$$

The term $\partial Z_i/\partial t$ is also known as the entrainment (McNaughton and Spriggs 1986). The combination of Equation 12 with Equation 11 results in an expression to determine $\partial Z_i/\partial t$ as a function of kinematic fluxes at the surface and at the top of the mixed layer, and γ_{θ_V}.

$$\frac{\partial Z_i}{\partial t} = \frac{1}{\gamma_{\theta_V} Z_i} \left[\left(\overline{w'\theta'_V}\right)_{sfc} - \left(\overline{w'\theta'_V}\right)_{Z_i} \right] \tag{13}$$

Another variable controlling the growth rate of the mixed layer depth is the strength of step change in virtual potential temperature at Z_i ($\Delta\theta_V$), see Figure 1. For a convective boundary layer with measurable $\Delta\theta_V$ at the capping inversion, the conservation of energy can be also defined in terms of the input of energy at the surface-atmosphere interface and entrainment as sgown in Equation 14.

$$Z_i \frac{\partial \theta_{V_m}}{\partial t} = \left(\overline{w'\theta'_V}\right)_{sfc} + \Delta\theta_V \frac{\partial Z_i}{\partial t} \tag{14}$$

For boundary layers with strong $\Delta\theta_V$ (e.g., $\Delta\theta_V > 2$ K), the temporal variations in $\Delta\theta_V$ are crucial requirements to properly simulate the changes in mixed layer depths (see Table 1 in Delonge and Fuentes 2012 to learn that for the continental tropical atmospheric boundary layer $1.4 \pm 0.9 < \Delta\theta_V < 2.0 \pm 1.4$ K, but values can reach up to 5 K). According to Tennnekes (1973) and Betts (1974), temporal variations in $\Delta\theta_V$ are governed by entrainment of heat into the mixed layer and warming of the mixed layer as defined in Equation 15.

$$\frac{\partial \Delta\theta_V}{\partial t} = \gamma_{\theta_V} w_e - \frac{\partial \theta_{V_m}}{\partial t} \tag{15}$$

The variable w_e represents the entrainment velocity, and once is multiplied by γ_{θ_V} causes $\Delta\theta_V$ to change. The w_e is normally defined (see Tennekes 1973, Betts 1974) as the difference between boundary layer growth rate ($\partial Z_i/\partial t$) and the average atmospheric subsidence ($\overline{w_s}$) as shown in Equation 16.

$$w_e = \frac{\partial Z_i}{\partial t} - \overline{w_s} \tag{16}$$

The $\overline{w_s}$ cannot be readily measured or estimated with single atmospheric column models. Instead, it is often derived from synoptic-scale calculations or regional numerical models. Based on regional numerical model calculations, $\overline{w_s}$ can vary from -0.03 to -0.01 m s^{-1}. It is a good practice to allow

$\overline{w_s}$ to vary depending on air mass type and cloudiness. By employing the budget relationships for slab-type models (Lilly 1968), the w_e can be estimated from knowledge of entrained kinematic heat fluxes into the mixed layer and the magnitude of $\Delta\theta_V$, see equation Equation 17.

$$w_e = -\frac{\left(\overline{w'\theta'_V}\right)_{Z_i}}{\Delta\theta_V} \tag{17}$$

The entrainment of kinematic heat flux at the top of the mixed layer (i.e., $(\overline{w'\theta'_V})_{Z_i}$) is ordinarily defined in terms of a fraction of surface fluxes as described in Equation 18.

$$-\left(\overline{w'\theta'_V}\right)_{Z_i} = \beta\left(\overline{w'\theta'_V}\right)_{sfc} \tag{18}$$

In Equation 18, the β represents a closure constant whose average values can range from 0.2 to 1.0. The theoretical origin for Equation 18 comes from the common observation that the kinematic virtual heat flux linearly decreases with altitude in the mixed layer (see Figure 6, Betts 1974).

To derive a prognostic algorithm for determining the mixed layer depth, it is necessary to estimate the temporal variations in $\Delta\theta_V$ and energy entrainment from aloft into the mixed layer. An analytical expression can be obtained for $\Delta\theta_V$ when atmospheric subsidence is neglected (i.e., $\overline{w_s} = 0$). By combining Equations 11 and 15 and making use of the closure assumption included in Equation 18, we obtain the results included in Equation 19.

$$\frac{\Delta\theta_V}{\partial t} = \gamma_{\theta_V}\frac{\partial Z_i}{\partial t} - \left(\overline{w'\theta'_V}\right)_{sfc}\left(\frac{1+\beta}{Z_i}\right) \tag{19}$$

To eliminate $(\overline{w'\theta'_V})_{sfc}$ in Equation 19 (just for mathematical purposes), with no subsidence, we make use of the definition included in Equation 17 and the closure assumption stated in Equation 18. The results $((\overline{w'\theta'_V})_{sfc} = (\Delta\theta_V/\beta)(\partial Z_i \partial t))$ are included in Equation 20.

$$Z_i\frac{\Delta\theta_V}{\partial t} = \gamma_{\theta_V} Z_i\frac{\partial Z_i}{\partial t} - \Delta\theta_V\left(\frac{1+\beta}{\beta}\right)\frac{\partial Z_i}{\partial t} \tag{20}$$

Upon rearranging and multiplying Equation 20 by $Z_i\beta^{-1}$, the following differential Equation 21 can be conveniently rewritten.

$$Z_i\beta^{-1}Z_i\frac{\Delta\theta_V}{\partial t} + \Delta\theta_V\left[1+\beta^{-1}\right]Z_i\beta^{-1}\frac{\partial Z_i}{\partial t} = \gamma_{\theta_V} Z_i\beta^{-1}\frac{\partial Z_i}{\partial t} \tag{21}$$

Equation 21 is a separable differential equation. The application of Leibniz's rule of integration can yield the analytical expression shown in Equation 22.

$$\frac{\partial}{\partial t}\left(Z_i^{\left[1+\beta^{-1}\right]}\Delta\theta_V\right) = \gamma_{\theta_V} Z_i^{\left[1+\beta^{-1}\right]}\frac{\partial Z_i}{\partial t} \tag{22}$$

For the analysis of Z_i in a given air mass, one can assume that γ_{θ_V} can mostly remain constant. Therefore, combining Equation 18 with Equations 11, 15, 17, and 18 can lead to the $\Delta\theta_V$ finite-difference expression shown below.

$$\Delta\theta_V(t)Z_i^{\left[1+\beta^{-1}\right]}(t) = \Delta\theta_V(t_0)Z_i^{\left[1+\beta^{-1}\right]}(t_0) + \frac{\gamma_{\theta_V}}{2+\beta^{-1}}\left(Z_i^{\left[2+\beta^{-1}\right]}(t) - Z_i^{\left[2+\beta^{-1}\right]}(t_0)\right) \tag{23}$$

The t_0 in Equation 23 refers to the initial time or time step considered in the estimation of $\Delta\theta_V$. Equation 23 can be employed to determine the temporal variations in $\Delta\theta_V$, making use of the initial conditions for Z_i and $\Delta\theta_V$ (i.e., $Z_i(t_0)$ and $\Delta\theta_V(t_o)$). It is important to recognize that two assumptions were considered in the derivation of Equaiton 23. The first assumption is that atmospheric subsidence is nil ($\overline{w_s} = 0$). The second one is that $\partial Z_i/\partial t \neq 0$. For those conditions when the growth of the mixed layer is almost in steady state (i.e., $\partial Z_i/\partial t \to 0$), as it happens during the later part of the afternoon, then the temporal variations in $\Delta\theta_V$ can be obtained from the solution of the differential Equation 15. The result is given below.

$$\Delta\theta_V(t) = \Delta\theta_V(t_0) - (\Delta\theta_{Vm}(t) - \Delta\theta_{Vm}(t_0)) \tag{24}$$

When initial conditions of the mixed layer are such that $Z_i(t) >> Z_i(t_0)$ (as occurs immediately after snrise), Equation 24 can be reduced to the Equation 25.

$$\Delta\theta_V(t) = \frac{\gamma_{\theta_V}}{2+\beta^{-1}}Z_i(t) \tag{25}$$

Summary

Numerous boundary layer entrainment algorithms exist to estimate the temporal variations of the mixed layer depth. As part of the Beltsville 2020 workshop, we identify and apply the most practical methods to determine the rates of energy entrainment into the mixed layer so that temporal variations in the mixed layer depth can be determined. We will use the three algorithms summarized below.

Algorithm I

In the absence of (i) atmospheric subsidence, (ii) heat entrainment into the mixed layer, and (ii) diminished wind shear conditions, McNaughton and Spriggs (1986) modified Equation 13 to accordingly define the growth rate of the mixed layer depth in terms of surface kinematic heat flux and the virtual potential temperture gradient above the mixed layer as shown in Equation 26. In addition, this model does not consider the influences of the strength of the capping inversion (i.e., $\Delta\theta_V = 0$).

$$\frac{\partial Z_i}{\partial t} = \frac{\left(\overline{w'\theta'_V}\right)_{sfc}}{\gamma_{\theta_V} Z_i} \tag{26}$$

Algorithm II

In environments experiencing atmospheric sinking motions, the McNaughton and Spriggs (1986) model can be modified to consider the influence of regional subsidence as shown in Equation 27.

$$\frac{\partial Z_i}{\partial t} = \frac{\left(\overline{w'\theta'_V}\right)_{sfc}}{\gamma_{\theta_V} Z_i} + \overline{w_s} \tag{27}$$

Algorithm III

Based on analyses of the turbulent kinetic energy (TKE) budget equation, Tennekes and Driedonks (1981) proposed an entrainment parameterization. For a convective boundary layer under the influences of negligible wind shear conditions, an approximation of the entrainment can be obtained by using Equation 28:

$$\frac{\partial Z_i}{\partial t} = \frac{C_K W_*^3}{C_T W_*^2 + \frac{g}{\theta_V} Z_i \Delta\theta_V} \tag{28}$$

C_K and C_T are empirical coefficients with the values of 0.18 and 0.8, respectively. The variable W_* is the convective velocity scale ($W_*^3 = [(g/\overline{\theta_V})(\overline{w'\theta'_V})_{sfc} Z_i]$). The $\overline{\theta_V}$ is the temporally averaged virtual potential temperature, g is gravitational acceleration, and $\Delta\Theta_V$ is the difference in temperature at Z_i and some infinitesimal distance above the mixed layer.

Data analyses

Available data

Surface energy balance flux data (**Cal_flux_data.txt**) are provided for a site located in the Sacramento San Joaquin River Delta (latitude of 38^o $06^{'}$ $32.61^{''}$ and longitude of 121^o $32^{'}$ $6.41^{''}$), California. The data file includes two periods: day of year (DOY) 150 to 180 (Period A) and 320 to 350 (Period B). These two periods include summer and fall time conditions.

Table 1: The data file **Cal_flux_data.txt** has the variables listed in the headings and includes sample values for the variables.

DecDOY	Time	Press	Tair	RH	Wspeed	Ustar	Rnet	H	LE	G
150.021	0.5	100.418	18.0	50.8	5.1	0.3	-84.6	-44.3	16.6	5.2
150.042	1.0	100.401	17.9	48.2	6.3	0.4	-86.6	-52.8	23.8	4.0
150.062	1.5	100.396	17.9	46.6	7.6	0.5	-88.3	-60.4	28.9	11.1

Names of variables are: DecDOY is decimal DOY, Time is decimal hour of day, Press is barometric pressure in kPa, Tair is ambient air temperature in ^{o}C, RH is the ambient relative humidity in %, Wspeed is the horizontal wind speed in m per s, Ustar is the friction velocity in m per s, Rnet is the net radiation in W per m^{-2}, H is the sensible heat flux in W per m^{-2}, LE is the latent heat flux in W per m^{-2}, and G is the soil heat flux in W per m^{-2}.

Data analyses and interpretation

For each period separately, perform the data analyses and create the plots enumerated below.

1. Calculate the sum of H, LE, and G and store the result in a new variable called *myRnet*. You need to ensure that mising data (i.e., **NaN**) are not included in the calculation.
2. For each meteorological of flux variable, compute the hourly average (μ) and standard deviation (σ).
3. Create a summary page of plots to display the statistics (i.e., $\mu \pm \sigma$) for all variables. Plot 1: temporal variation of Tair (left y axis) and RH (right y axis), with time of day on the x axis; plot 2: temporal variation of Wspeed (left y axis) and Ustar (right y axis); plot 3: temporal variation of averaged Rnet, H, LE, and G (left axis); plot 4: raw Rnet (left y axis) versus *myRnet*. For plot 4, add the 1:1 line.
4. For plot 4, determine the linear regression of Rnet versus *myRent*, forcing the regression to go through the origin. Also, estimate the coefficient of determination (R^2) and put the R^2 value on the plot.
5. Study plot 3 and identify periods of the day when closure of the suface energy balance is not attained (the surface energy balance ordinarily attains closure when the sum of H, LE, and G matches the measured Rnet values). Explain the likely reasons for the lack of surface energy closure.

6. Study plot 4 and derive an estimate of surface energy budget closure. Also, identify the likely processes that cannot be realistically captured with the measurements of surface energy balance components.

Numerical modeling and interpretation

The three algorithms outlined above need to be applied to estimate the diurnal patterns of the mixed layer. Two sets of simulations need to be done. One set of simulations is for Period A (DOY 150 to 180). The second set of simulations is for Period B (DOY 320 to 350). Simulation intial conditions are included in Table 2.

Table 2: This table provides the initial conditions for the six simulations to be done for each period (i.e., Period A and Period B) identified above. The end and start times of the simulations correspond to the hour of the day included in the rawdata file **Cal_flux_data.txt**.

Algorithm	Start time (h)	End time (h)	$Z_i(t_0)$ (m)	γ_{θ_V} (K km^{-1})	$\Delta\theta_V$(K)	$\overline{w}$ (m s^{-1})
I	7.0	17.0	100.0	6.0	0.0	0.0
I	7.0	1 7.0	100.0	12.0	0.0	00
II	7.0	17.0	100.0	6.0	0.0	-0.1
II	7.0	17.0	100.0	12.0	0.0	-0.1
III	7.0	17.0	100.0	6.0	1.0	0.0
III	7.0	17.0	100.0	12.0	1.8	0.0

1. For the cases listed in Table 2 and using the results of the data analyses obtained above, write Python code to simulate temporal variations of the convective mixed layer depth ($Z_i(t)$)
2. Plots the $Z_i(t)$ results on a single page. Three plots can be created. Plot 1: Averaged Rnet and H (on the y axis) versus time of day (on the x axis), from 6 to 18 hours. Plot 2: $Z_i(t)$ (on the y axis) versus time of day for the first four cases listed in Table 2. Plot 3: $Z_i(t)$ (on the y axis) versus time of day for the last two cases listed in Table 2. All plots need to have appropriate labels to denote the lines and symbols associated with $Z_i(t)$ for each method.
3. Study plot 2 to learn the differences in the estimated $Z_i(t)$. Explain why different values of γ_{θ_V} contribute to dissimilar temporal patterns of $Z_i(t)$. Explain the likely reasons for the different results.
4. Study plot 2 to learn the differences in the estimated $Z_i(t)$. Explain why different values of $\overline{w_s}$ contribute to dissimilar temporal patterns of $Z_i(t)$. Explain the likely reasons for the different results.
5. Study plot 3 to learn the differences in the estimated $Z_i(t)$ employing the TKE concepts. Explain why different values of $\Delta\theta_V$ contribute to dissimilar temporal patterns of $Z_i(t)$. Explain the likely reasons for the different results.
6. Contrast the the $Z_i(t)$ results for Period A and Period B. Explain why the results differ so much. While interpreting the $Z_i(t)$ results it is important to refer to the Rnet and H data.